Journal of Power Sources 278 (2015) 458–463

Contents lists available at ScienceDirect

Journal of Power Sources

journal homepage: www.elsevier.com/locate/jpowsour

Platinum supported on mesoporous carbon as cathode catalyst for direct methanol fuel cells

Mariano M. Bruno [a, b], Federico A. Viva [a, *], M. Agustina Petruccelli [a], Horacio R. Corti [a, c]

[a] Grupo Celdas de Combustible, Departamento de Física de la Materia Condensada, Centro Atómico Constituyentes, Comisión Nacional de Energía Atómica (CNEA), Av. General Paz 1499 (1650), San Martín, Buenos Aires, Argentina
[b] Escuela de Ciencia y Tecnología, Universidad Nacional de Gral. San Martín, Martin de Irigoyen 3100 (1650), San Martín, Buenos Aires, Argentina
[c] Instituto de Química Física de los Materiales, Medio Ambiente y Energía (INQUIMAE), Facultad de Ciencia Exactas y Naturales, Universidad de Buenos Aires, Intendente Güiraldes 2160 (1428), Ciudad Universitaria, Buenos Aires, Argentina

HIGHLIGHTS

- Pt nanoparticles supported on mesoporous carbon as cathode catalyst for DMFC.
- Improved nanoparticles distribution over the mesoporous carbon.
- Polarization measurements of active feed fuel cell.
- Higher peak power density for Pt/MC than Pt/C.
- Lower O_2 flow needed for Pt/MC to exceed Pt/C performance.

ARTICLE INFO

Article history:
Received 17 September 2014
Received in revised form
19 December 2014
Accepted 20 December 2014
Available online 23 December 2014

Keywords:
Mesoporous carbon
Pt catalyst
Oxygen reduction reaction
Direct methanol fuel cells

ABSTRACT

Platinum nanoparticles supported on mesoporous carbon were obtained by an impregnation and reduction method with $NaBH_4$ as the reducing agent. The high specific surface area mesoporous carbon was obtained by carbonization of a resorcinol-formaldehyde polymer with a cationic polyelectrolyte as a soft template. Surface characterization performed by transmission electron microscopy and powder X-ray diffraction showed a homogeneous distribution and high dispersion of the metal particles on the mesoporous support. The carbon-supported Pt catalyst was employed as cathode catalyst in a direct methanol fuel cell where a 30% increase in power density was obtained when compared to Pt supported on Vulcan carbon, under the same conditions.

1. Introduction

Proton exchange membrane fuel cells (PEMFCs) are electrochemical devices proposed as a convenient power source for stationary and portable applications. Particularly, direct methanol fuel cells (DMFC) have showed the advantages of using a fuel with high volumetric energy density, easy handling, transport and operation [1–3]. However, the commercial viability of the DMFCs technology has been hindered by several challenges like the sluggish methanol oxidation and the methanol crossover through the membrane. Pt catalyst has been recognized as the best catalysts for oxygen reduction reaction (ORR) for the cathode of DMFCs [4,5]. However, the low Pt natural abundance, and therefore high cost, together with a complex reaction kinetic are drawbacks that must be overcome.

The use of a catalyst support has been proved to be an effective approach to lower the loading of noble metal in the catalysts and improve the catalytic mass activity [6–8]. In this regard, the preparation of particles with homogeneous size and dispersion, while reducing the Pt loading emerged as a solution to increase the catalytic mass efficiency [9]. Hence, synthesis conditions of Pt or Pt alloys nanoparticles as electrocatalytic materials possessing the aforementioned properties, have become of paramount importance [10,11]. The physical and chemical properties of the carbon support affect the structure and properties of the catalyst [12]. Carbon black, like Vulcan XC-72R, has been for long the material most commonly

* Corresponding author.
E-mail address: viva@tandar.cnea.gov.ar (F.A. Viva).

http://dx.doi.org/10.1016/j.jpowsour.2014.12.097
0378-7753/

used as support in the preparation of commercial electrocatalysts for fuel cells [13]. Nonetheless, other types of carbon morphologies have been studied to improve the characteristics offered by carbon Vulcan XC-72R as support [14]. These include: carbon nanotubes, carbon nanofibers, carbon nanocoils, ordered carbons and macroporous carbons just to mention the most used [14–16]. High specific surface area in combination with a large number of anchoring sites of the carbon support provides highly dispersed particles of small size. However, a high specific surface area is associated with small pore sizes, which may not be advantageous. It is known that perfluorosulfonate-ionomer (Nafion) cannot penetrate into pores smaller than 20 nm [17–19]. Consequently, Pt nanoparticles deposited into these pores can become unavailable to participate in establishing a triple phase boundary [17,20]. Furthermore, small size pores provide inefficient mass transport for the reactants and products [18,19], suggesting that tailoring the carbon structure is necessary to achieve the best catalyst performance.

Structured carbons have emerged as promising materials to meet the aforementioned challenge [21–23] by adjusting the pore structure according to the one needed by the application [24,25]. In this sense, the porous material structure must provide an adequate substrate for nanoparticle anchoring, facilitate reactants mass transport and posses water handling capability for removing water generated at the cathode [26,27]. Although promising results were found for several structured carbon materials as supports, there is still information lacking about the best morphological structure of carbon supports on the cathode side of DMFCs, as well as the optimized methods to prepare MEAs with the structured carbon supported catalyst.

In this work, carbon with a pore size distribution centered at 20 nm was used as the catalyst support. The mesoporous carbon (MC) was obtained by carbonization of a structured resorcinol formaldehyde polymer, using a cationic polyelectrolyte as a structuring agent [28]. Specific surface area and pore size distribution of the carbon support were determined by nitrogen adsorption isotherm. Platinum nanoparticles supported on mesoporous carbon were obtained by the impregnation and reduction method with $NaBH_4$ as a reducing agent in basic aqueous media. Transmission electron microscopy (TEM) and powder X-ray diffraction (PXRD), as well as electrochemical surface area measurement, were employed for the catalyst nanoparticles characterization. Finally, the performance of membrane electrode assembly (MEA) prepared with Pt nanoparticles supported on the MC as cathode catalyst of a DMFC was measured and compared against Pt deposited on Vulcan carbon by the same procedure.

2. Experimental

2.1. Mesoporous carbon preparation

Mesoporous carbon support was obtained using the method described elsewhere [29]. In brief, a precursor was prepared by polymerization of resorcinol (Fluka) and formaldehyde (Cicarelli, 37 wt %). Sodium acetate (Cicarelli) was used as catalyst, and a cationic polyelectrolyte (polydiallyl-dimethylammonium chloride, PDADMAC, Sigma–Aldrich) was used as a structuring agent. The reactive mixture of resorcinol (R), formaldehyde (F), and sodium acetate (C) was stirred at 40 °C for 10 min before the addition of PDADMAC (P) in a molar ratio of 1:3:0.04:0.03 (R:F:C:P), respectively. Once the mixture became homogeneous, the solution was heated to 70 °C for 48 h at atmospheric pressure. The resulting brown R–F piece was dried in air for 3 days. The polymer was then carbonized under nitrogen stream in a tubular furnace from ambient temperature to 1000 °C at a heating rate of 40 °C/h. Finally, the material was grinded and passed through a 40 μm pore sieve. An ASAP 2020 (Micrometrics) instrument was used to measure the nitrogen adsorption–desorption isotherms at −196 °C. The t-plot and Brunauer–Emmett–Teller (BET) methods were used to determine the micropores volume and the specific surface area, respectively. The pore size distribution was obtained from the desorption branch of the nitrogen isotherm by the Barrett–Joyner–Halenda (BJH) method.

2.2. Catalyst preparation

A solution of Pt metal precursor ($H_2PtCl_6 \cdot 6H_2O$, Tetrahedron) was added in a calculated amount to the slurry of the MC in order to achieve a metal loading of 40% w/w. The pH was adjusted to 8 with 1 M NaOH solution (Pro Analysis, Merck). The dispersion was heated at 80 °C. Then, $NaBH_4$ (granular 98%, Sigma–Aldrich) was added in a molar ratio $NaBH_4$ to metal salt of 5:1, and the temperature was maintained for an additional 2 h, followed by stirring for 12 h. The solid was separated by centrifugation, and it then was successively washed until the supernatant solution showed a neutral pH and absence of Cl^- by reaction with $AgNO_3$ (saturated solution). Pt supported on Vulcan carbon (Vulcan XC-72, Cabot) was prepared following the same procedure described above. The Vulcan was previously washed by boiling it in 30 wt % HCl aqueous solution.

2.3. Catalyst characterization

Powder X-ray diffraction pattern of the catalyst was obtained using a Siemens D5000 diffractometer with a Cu Kα source operating at 40 kV and 30 mA. The angle extended from 20° to 100° with a step size of 0.02° and a counting time of 2 s. Transmission electron microscope images were acquired with a Philips CM200, while energy dispersive X-ray spectrometry (EDS) was performed using an EDAX DC X4 to confirm the presence of Pt and the absence of other metals.

Thermogravimetric analyses (TGA) were performed with a Shimadzu TGA-51 instrument. Supported catalyst samples (5–10 mg) were heated up to 1000 °C at 5 °C per minute on a titanium crucible in air atmosphere (flow: 100 cm^3 min^{-1}). The metal content of the supported catalysts were calculated from the difference between the initial and final weights.

2.4. Electrochemical surface area (ECSA) determination

In order to determine the electroactive Pt surface area, CO stripping voltammetry was performed. A suspension of the supported catalyst was prepared and spread over the working electrode (WE), which contained a glassy carbon (SPI) disk 5 mm in diameter mounted in a Teflon rod connected through a gold wire. The Pt nanoparticles supported on the MC (Pt/MC) and on Vulcan carbon (Pt/C) were analyzed. The exposed face of the WE was sanded with 400 grit paper to get a rough surface before it was covered with the suspension. The CO stripping was performed in a double walled electrochemical cell with three electrodes and the temperature was maintained at 25.0 °C with a Tempunit TU-16D (Techne) temperature controller. The counter electrode (CE) consisted of a coiled Pt wire 0.5 mm in diameter and 30 cm length, whereas a Ag/AgCl (sat. KCl) electrode was used as a reference electrode (RE). All potentials were converted against the standard hydrogen electrode (SHE). A 0.5 M H_2SO_4 (95–97 %, Merck) solution was saturated with carbon monoxide (RG 4.8, Indura) for 60 min to allow the complete coverage of CO onto the catalyst surface, while maintaining the working electrode potential at 0.25 V vs. SHE. The excess CO in the solution was purged with N_2 (RG 4.8, Indura) gas for 15 min at a constant potential of 0.25 V vs. SHE. Finally, the

stripping voltammograms were recorded between 0.05 and 1.0 V vs. SHE with a scan rate of 1 mV s^{-1} at 25 °C.

2.5. MEA preparation and fuel cell testing

Pt/MC and Pt/C were used as the cathode catalyst, while PtRu/C 60% w/w (Fuel Cell Store) was used as the anode catalyst. The cathode was prepared as described below. The catalyst suspension was prepared by mixing the catalyst with milli-Q water and Nafion ionomer solution (5% w/w, Ion Power) in a 1:3:1 proportion by weight, and spread on one side of a 5 cm^2 Toray C paper TGP–H 60 10% PTFE coated (Fuel Cell Technologies). The electrode loading was ca. 3 mg cm^{-2}. A Nafion 212 membrane (Ion Power) was placed between the electrodes and then hot pressed at 150 °C and 40 bar for 25 min. The Nafion membrane was previously treated by boiling in H_2O_2 3% w/w (H_2O_2 30% w/w, Biopack) followed by H_2SO_4 3% w/w (95–97 % w/w, Merck). After assembling the cell, the MEA was re-humidified by circulating water overnight at 80 °C. Galvanodynamic polarization tests were performed at 60 °C from the open circuit voltage (OCV) to a voltage close to short circuit (0.05 V). The measurements were performed with an Autolab PGSTAT302N potentiostat equipped with a 20A booster. The cell was fed with 1 M methanol (Merk, HPLC grade) aqueous solution through the anode. The anode was fed by a peristaltic pump at a flow rate of 2.0 cm^3 min^{-1}. At the cathode, air (RG 3.0, Indura) or oxygen (RG 4.8, Indura) at ambient pressure with flow rates from 50 to 150 sccm were supplied without humidification. The flow rate of the gas was regulated and measured by a mass flow controller (Allicat). Current collectors with pin type flow field (manufactured *in house*) were used at both sides of the cell.

3. Results and discussion

3.1. Carbon support and catalyst surface characterization

The N_2 adsorption–desorption isotherm and pore size distribution (inset) are shown in Fig. 1. The calculated BET specific surface area of the MC is almost three times higher than the one for Vulcan carbon (600 m^2 g^{-1} vs. 235 m^2 g^{-1}). The pore size distribution (BJH-desorption branch) presents a high and narrow peak centered at 20 nm for MC and a much broader and low peak centered at 30 nm for the Vulcan carbon. Moreover, the calculated total pore volume (partial pressure P/P_o = 0.99) for MC resulted in 1.00 cm^3 g^{-1} indicating a higher porosity than Vulcan carbon with a value of 0.44 cm^3 g^{-1} (P/P_o = 0.99). In addition, the micropore volume was calculated resulting in a value of 0.10 cm^3 g^{-1} for MC and 0.01 cm^3 g^{-1} for Vulcan carbon. Previous reports have described the morphological characteristics of the MC [28–31]. It was shown that in order to obtain the high surface area in conjunction with the served values of pore and micropore volume, the MC must consist of porous uniform spheres clustered in a fairly regular array [30,31], yielding a hierarchical pore structure (micro and mesoporosity). The micropores on the carbon surface have been proposed as optimal anchoring sites for the catalyst nanoparticles [32,33], in addition to improve the reactant mass transport to/from the catalyst region [13,34].

The PXRD patterns of the prepared catalysts are shown in Fig. 2. The diffractograms show the characteristic diffraction peaks of face centered cubic (fcc) crystalline Pt [35] corresponding to the planes (111), (200), (220), and (311). The Pt/MC's peaks in the diffractogram are wider compared to those of the Pt/C catalyst, indicating smaller crystallites. The lattice parameters were calculated by indexing the first three peaks, that is, (111)-(200)-(220), yielding a value of 0.392 ± 0.001 nm for Pt/MC and for Pt/C, while the crystal sizes were calculated using Scherrer's formula [36] giving a value of 6.1 nm ± 0.5 nm for Pt/MC and 7.6 ± 0.5 nm for Pt/C.

Dispersion and size of metal nanoparticles on the two carbon supports were assessed by TEM images, as shown in Fig. 3. Low-magnification TEM images show a better dispersion of catalyst particles across the support for MC (Fig. 3A) than for carbon Vulcan (Fig. 3D). Fig. 3(B, E) shows images at higher magnifications used for the size diameter determination of Pt in each support. The catalyst particle size diameter distribution was obtained by measuring the diameter of 200 randomly selected particles. Fig. 3(C, F) represents the bar plots of the particle size diameter measured for Pt/MC and Pt/C, respectively. Both catalysts exhibit, for the particle size diameter, a Gaussian distribution; however, Pt/MC shows a narrow dispersion of the particle diameter with a mean value of 5.3 nm, compared to Pt/C which presents a mean value of 6.8 nm, and exhibits particles with sizes up to 17 nm. The wide dispersion of particles including clusters as well as small particles (<2 nm) can be observed in Fig. 3E across the Vulcan support.

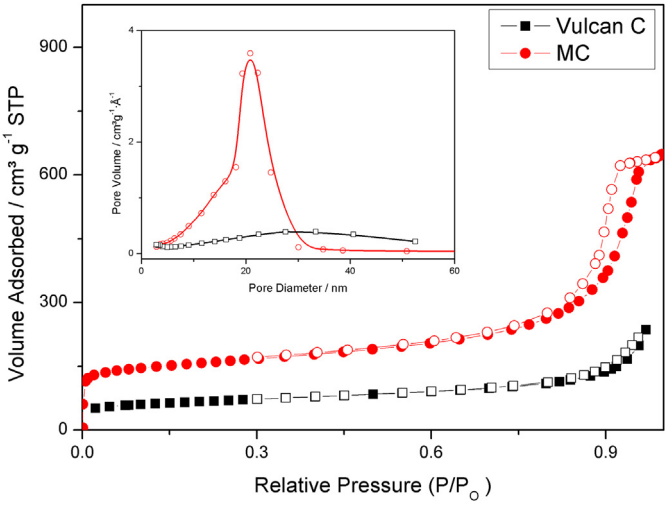

Fig. 1. Nitrogen adsorption–desorption isotherms at −196 °C for MC and Vulcan carbon Inset: Pore size distribution. Filled marker: adsorption branch; hollow marker: desorption branch.

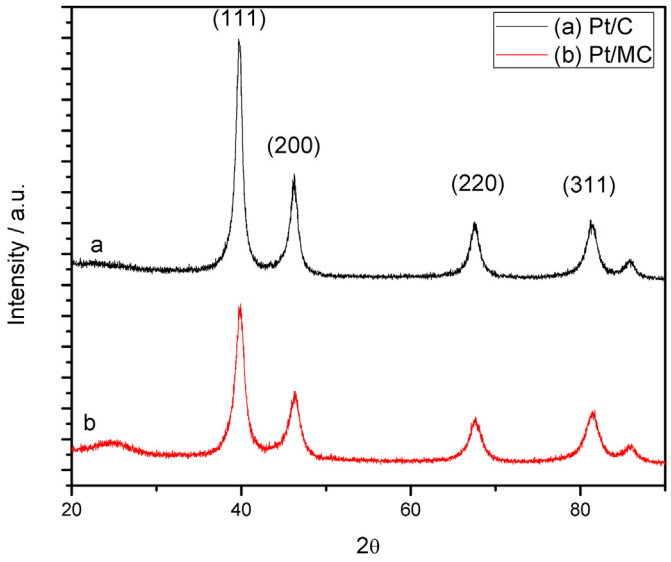

Fig. 2. X-ray diffraction pattern of Pt/MC and Pt/C.

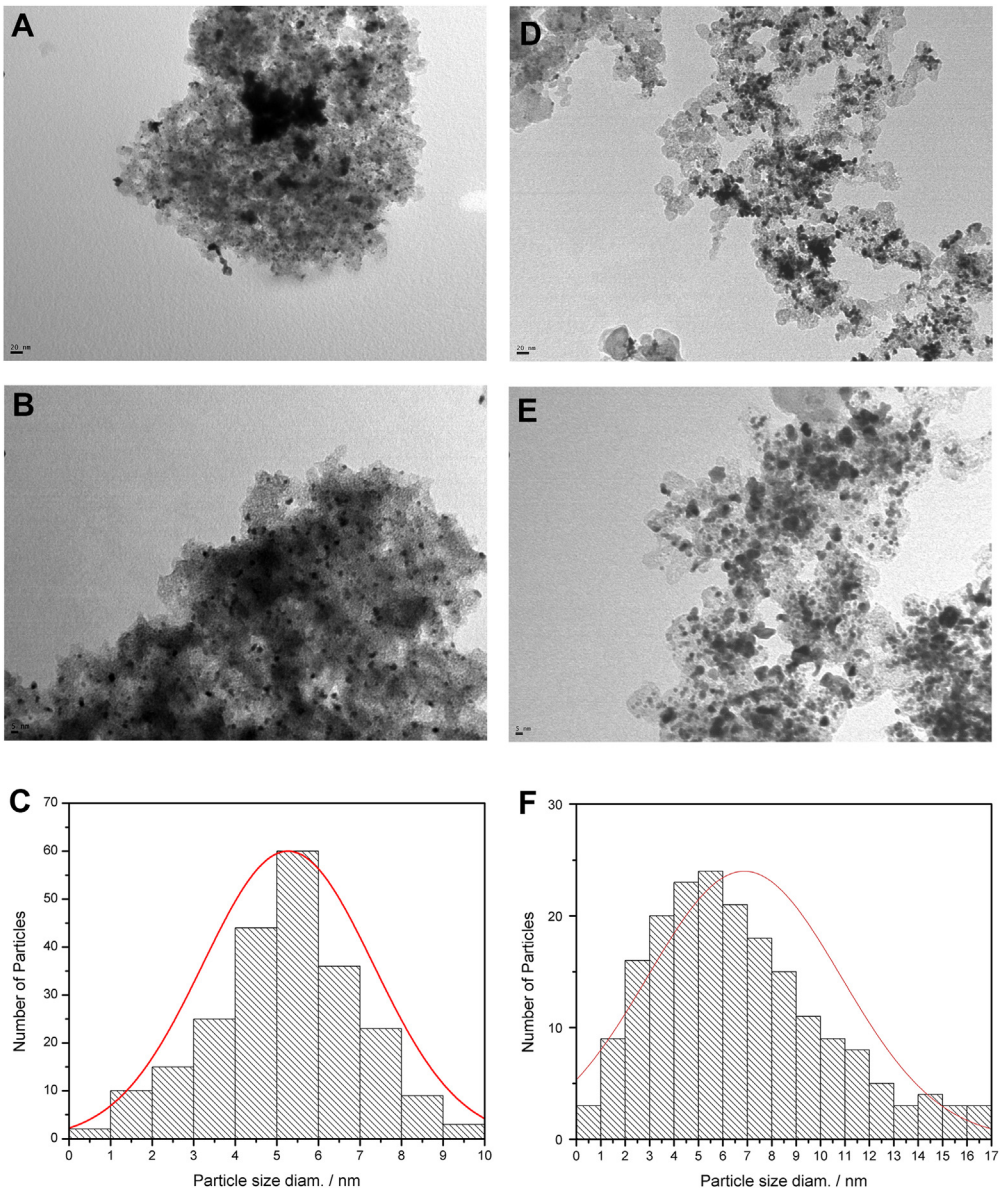

Fig. 3. A), B) and C) TEM images of Pt/MC at different magnification and particles size distribution with the corresponding histogram. D), E) and F) TEM images of Pt/C at different magnification and particles size distribution with the corresponding histogram.

TGA was employed to determine the final loading of metallic Pt on the carbon support. The measurements indicated a value of 35% w/w for Pt/MC and 37% w/w for Pt/C, these results being in close proximity to the nominal amount used during the synthesis (40% w/w).

3.2. Electrochemical surface area

ECSA of both supported catalysts were calculated from the CO stripping sweeps. In order to determine the CO oxidation charge, the second CV scan was used as background current and a charge of 420 μC cm^{-2} was assumed as the oxidation charge for one monolayer of CO on a smooth Pt surface. Fig. 4 shows the cyclic voltammogram of Pt/MC and Pt/C in 0.5 H_2SO_4 showing the oxidation of CO adsorbed onto the catalysts surface. The catalyst onto Vulcan carbon exhibits a slightly lower electrooxidation onset potential than that on MC, indicating a more facile CO oxidation. The calculated ECSAs values were 66 $m^2 g^{-1}$ for Pt/MC and 38 $m^2 g^{-1}$ for Pt/C, representing a two-fold increase by the use of MC. These results reflect the effect of the MC support on the particle formation and distribution during the synthesis process.

3.3. Fuel cell characterization

Polarization measurements of the fuel cells with Pt/MC and Pt/C as cathode catalyst at 60 °C were performed. In order to evaluate the best conditions of the oxygen and air feeding at the cathode side, galvanodynamic linear sweep voltammetry measurements were carried out at different flows while keeping constant the methanol concentration and the temperature. Fig. 5(A, B) show the polarization and power plots at different O_2 flows for Pt/MC and Pt/C. Both catalysts present an OCV around 0.7 V. Under load, the cells with catalysts supported on MC and Vulcan showed different behaviors. The cell with Pt/C showed a larger initial voltage drop than Pt/MC, and a slightly higher internal resistance as observed in the ohmic polarization region. At high load, in the mass transport

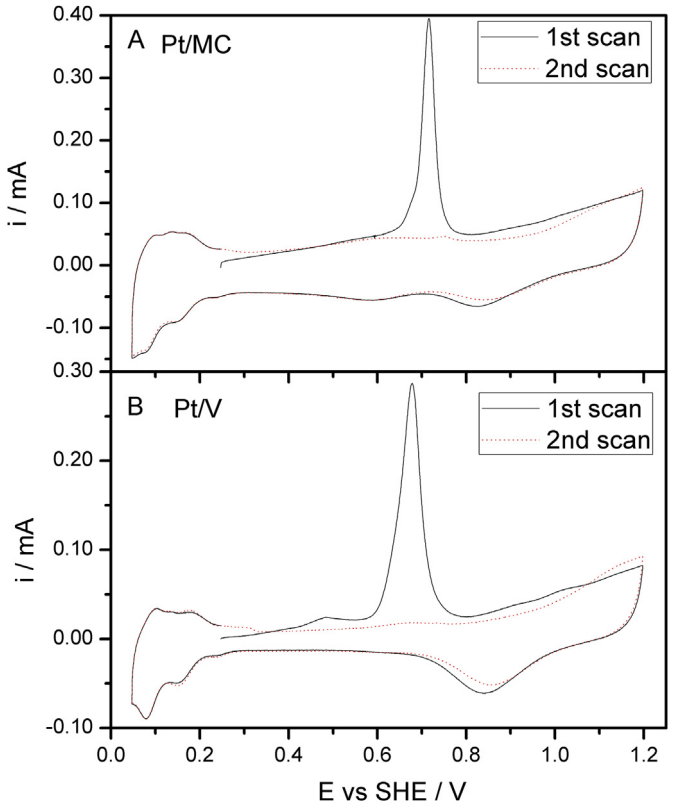

Fig. 4. CO stripping voltammograms in 0.5 H_2SO_4 at 1 mV s^{-1}. A) Pt/MC. B) Pt/C.

while the cell with Pt/MC showed a maximum power density at a flow of 100 sccm, as indicated above, and then for 150 sccm the power density decrease to a value close to 70 sccm. Some authors have presented the cell performance behavior under different measurement conditions for DMFC [37–41]. Generally, the performance improves with the O_2 flow rate up to a value where it either stays constant or slightly decreases again, as observed by other authors [39]. In this study, such behavior was observed for the Pt/MC at lower flows than the ones usually required; i. e. at flows where the performance of the cell is still rising. The Pt/MC behavior suggest that the support, due to the carbon hierarchical pore distribution and high surface area, promotes, what we call, a drying effect of the catalytic layer with the increase of oxygen flow and therefore a decrease in the cell performance. This drying effect is not a total dry-out of the catalytic layer, but a decrease in the water content, which affects the three phase boundary region and is particularly noticeable at high current density, i.e. in the mass transport region. Fig. 6(A, B) show the polarization and power plots at different air flows at the cathode for Pt/MC and Pt/C. Again, the fuel cell with mesoporous carbon as support had the best performance. Although power density is lower than when fed with oxygen, as expected, a similar behavior with respect to the flow rate was found. For Pt/C, the performance improved with increasing air flow in the same way as with the O_2 flow increase. In the case of Pt/MC the voltage and power density for 100 sccm and 150 sccm (Fig. 6A) present similar values up to a current density of 120 mA cm^{-2}. At higher current density values, the voltage and power density for the 100 sccm flow shows higher values than that of 150 sccm. The role that the aforementioned drying effect plays in the case of using air in the cathode is more difficult to explain and

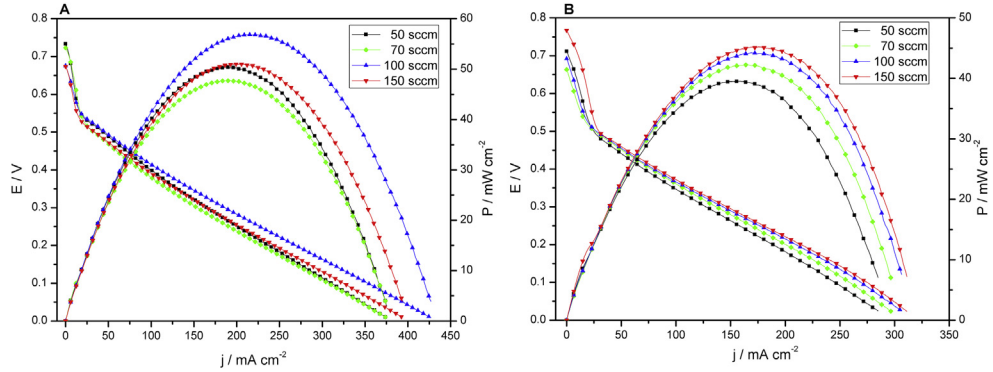

Fig. 5. Polarization and power curves at different O_2 flows for A) Pt/MC and B) Pt/C at 60 °C and 1 M methanol as anode fuel.

region, the characteristic voltage drop at high current density is slightly observed for the cell with Pt/C catalyst. On the other hand, for the cell with Pt/MC as cathode catalyst, the voltage drop due to reactant starvation is unnoticeable. This improved handling of reactants in the mass transport region was observed also for a DMFC with the mesoporous carbon as support for PtRu in the anode side [34], indicating that the use of mesoporous carbon as support for cathode or anode catalyst improved the overall performance of the DMFC. Fuel cell with Pt/MC as cathode showed a better power density than that with Pt/C for all the different oxygen flows measured. The maximum power density reached by the Pt/MC was 58 mW cm^{-2} at an O_2 flow of 100 sccm while the Pt/C reached 45 mW cm^{-2} at a higher O_2 flow (150 sccm). The cells with Pt/MC and Pt/C showed a different behavior when the oxygen flow was increased. The cell with Pt/C had a progressive increase of the maximum power density as the oxygen flow was incremented, this can be related to the lower fraction of O_2 in the dry gas stream. The air flowing through the cathode has a higher drying effect than pure O_2 for a given flow, since the amount of oxidant is lower and consequently less water is produced.

Overall, for a cathode half-cell fed either with O_2 or air, Pt/MC requires lower flow rates than Pt/C to attain the peak performance.

4. Conclusions

The results obtained in this study show that the mesoporous carbon used as support improved the catalyst dispersion. Pt nanoparticles of 5.3 nm in size were obtained on MC, which is, on average, 25% smaller than those formed on Vulcan carbon under the same synthesis conditions.

Polarization measurements of DMFCs showed that Pt/MC had a better performance compared with Pt/C as cathode catalyst. The

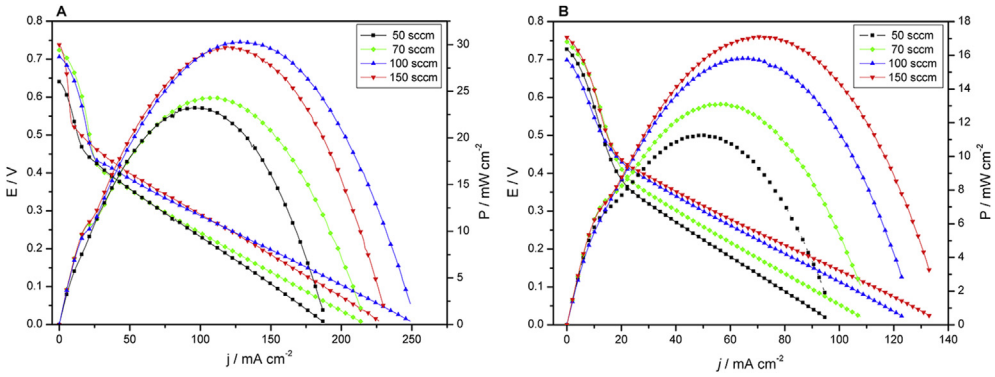

Fig. 6. Polarization and power curves at different Air flows for A) Pt/MC and B) Pt/C at 60 °C and 1 M methanol as anode fuel.

oxygen feeding of the fuel cells with MC showed an increase in the performance up to 100 sccm (best operation condition), followed by a drop in the power density at higher flow. Pt/MC diminishes the mass transport losses promoting the water transportation. However, this property also promotes the drying out of the MEA at high flow rates.

Mesoporous carbon has been demonstrated as a suitable cathode catalyst support for DMFC. The obtained results indicate that a catalyst on a MC support requires different MEA preparation and cell operation conditions as compared with the typical ones employed with metal nanoparticles catalyst supported on Vulcan carbon. Therefore, nanostructured materials result in a promising material for DMFC, but it is worth to be mentioned that a careful searching of the best conditions of MEA preparation and operation for each support proposed is necessary in order to take advantage of it.

Acknowledgments

The authors thank for financial support from Agencia Nacional de Promoción Científica y Tecnológica (ANPCyT) (PICT 008-2009 PRH200-4), Concejo Nacional de Investigaciones Científicas y Tecnológicas (CONICET (PIP 095)) and Universidad Nacional de Gral. San Martin (UNSAM) (SJ10/04). MMB, FAV and HRC are permanent research fellows of CONICET.

References

[1] M.M.P. Jansen, J. Moolhuysen, Electrochim. Acta 21 (1976) 869–878.
[2] S. Surampudi, S.R. Narayanan, E. Vamos, H. Frank, G. Halpert, A. Laconti, J. Kosek, G.K.S. Prakash, G.A. Olah, J. Power Sources 47 (1994) 377–385.
[3] D. Edlund, Methanol Fuel Cell Systems: Advancing towards Commercialization, first ed., Pan Stanford Publishing, 2011.
[4] H.A. Gasteiger, S.S. Kocha, B. Sompalli, F.T. Wagner, Appl. Catal. B 56 (2005) 9–35.
[5] A. Rabis, P. Rodriguez, T.J. Schmidt, ACS Catal. 2 (2012) 864–890.
[6] Z. Cui, C. Liu, J. Liao, W. Xing, Electrochim. Acta 53 (2008) 7807–7811.
[7] J. Figueiredo, M. Pereira, P. Serp, P. Kalck, P. Samant, J. Fernandes, Carbon 44 (2006) 2516–2522.
[8] H. Liu, C. Song, L. Zhang, J. Zhang, H. Wang, D. Wilkinson, J. Power Sources 155 (2006) 95–110.
[9] V. Mehta, J.S. Cooper, J. Power Sources 114 (2003) 32–53.
[10] M. Shao, A. Peles, K. Shoemaker, Nano Lett. 11 (2011) 3714–3719.
[11] F. Maillard, Electrochim. Acta 47 (2002) 3431–3440.
[12] F. Rodríguez-Reinoso, Carbon 36 (1998) 159–175.
[13] M.M. Bruno, F.A. Viva, Carbon materials for fuel cells, in: H.R. Corti, E.R. Gonzalez (Eds.), Direct Alcohols Fuel Cells, Springer Netherlands, Dordrecht, 2014, pp. 231–270.
[14] A.L. Dicks, J. Power Sources 156 (2006) 128–141.
[15] H.-Y. Du, C.-H. Wang, H.-C. Hsu, S.-T. Chang, S.-C. Yen, L.-C. Chen, B. Viswanathan, K.-H. Chen, J. Mater. Chem. 21 (2011) 2512–2516.
[16] X. Sun, M.S. Saha, Nanotubes, nanofibers and nanowires as supports for catalysts, in: J. Zhang (Ed.), PEM Fuel Cell Electrocatalysts and Catalyst Layers: Fundamentals and Applications, Springer, New York, 2008, pp. 655–704.
[17] V. Rao, P.A. Simonov, E.R. Savinova, G.V. Plaksin, S.V. Cherepanova, G.N. Kryukova, U. Stimming, J. Power Sources 145 (2005) 178–187.
[18] M. Uchida, Y. Fukuoka, Y. Sugawara, N. Eda, A. Ohta, J. Electrochem. Soc. 143 (1996) 2245–2252.
[19] M. Uchida, Y. Fukuoka, Y. Sugawara, H. Ohara, A. Ohta, J. Electrochem. Soc. 145 (1998) 3708–3713.
[20] M. Watanabe, H. Uchida, N. Ikeda, W. Kautek, M. Sahre, D.M. Soares, M. Uchida, Y. Fukuoka, Y. Sugawara, N. Eda, A. Ohta, J. Electrochem. Soc. 143 (1996).
[21] Y. Qiao, C.M. Li, J. Mater. Chem. 21 (2011) 4027–4036.
[22] J. Zeng, C. Francia, M.A. Dumitrescu, A.H.A.M. Videla, V.S. Ijeri, S. Specchia, P. Spinelli, Ind. Eng. Chem. Res. 51 (2012) 7500–7509.
[23] D. Banham, F. Feng, T. Fürstenhaupt, K. Pei, S. Ye, V. Birss, J. Power Sources 196 (2011) 5438–5445.
[24] M.M. Bruno, H.R. Corti, J. Balach, N.G. Cotella, C.A. Barbero, Funct. Mat. Lett. 2 (2009) 135.
[25] N. Veizaga, J. Fernandez, M. Bruno, O. Scelza, S. de Miguel, Int. J. Hydrog. Energ. 37 (2012) 17910–17920.
[26] S. Hoon, C. Pak, D. Jong, S.-A. Lee, H. Ik, J. Man, H. Chang, D. Seung, Electrochim. Acta 52 (2006) 1618–1626.
[27] J. Marie, R. Chenitz, M. Chatenet, S. Berthon-Fabry, N. Cornet, P. Achard, J. Power Sources 190 (2009) 423–434.
[28] M.M. Bruno, N.G. Cotella, M.C. Miras, C.A. Barbero, Colloids Surfaces A 362 (2010) 28–32.
[29] F.A. Viva, M.M. Bruno, M. Jobbágy, H.R. Corti, J. Phys. Chem. C 116 (2012) 4097–4104.
[30] S. Gavalda, K.E. Gubbins, Y. Hanzawa, K. Kaneko, K.T. Thomson, Langmuir 18 (2002) 2141–2151.
[31] M.M. Bruno, E.A. Franceschini, G.A. Planes, H.R. Corti, J. Appl. Electrochem. 40 (2010) 257–263.
[32] M.A. Fraga, E. Jordão, M.J. Mendes, M.M.A. Freitas, J.L. Faria, J.L. Figueiredo, J. Catal. 209 (2002) 355–364.
[33] F. Rodríguez-Reinoso, P. Santana, E.R. Palazon, M.A. Diez, H. Marsh, Carbon 36 (1998) 105–116.
[34] M.M. Bruno, M.A. Petruccelli, F.A. Viva, H.R. Corti, Int. J. Hydrog. Energ. 38 (2013) 4116–4123.
[35] D. Chu, S. Gilman, J. Electrochem. Soc. 143 (1996) 1685–1690.
[36] Z. Liu, X.Y. Ling, X. Su, J.Y. Lee, J. Phys. Chem. B 108 (2004) 8234–8240.
[37] M.A. Abdelkareem, N. Nakagawa, J. Power Sources 165 (2007) 685–691.
[38] Y.-D. Kuan, S.-M. Lee, M.-F. Sung, J. Fuel Cell Sci. Tech. 6 (2008) 011004.
[39] S.H. Seo, C.S. Lee, Energy Fuels 22 (2008) 1212–1219.
[40] N. Nakagawa, Y. Xiu, J. Power Sources 118 (2003) 248–255.
[41] A. Casalegno, R. Marchesi, F. Rinaldi, J. Fuel Cell Sci. Tech. 4 (2006) 418–424.